W. Fundamenski, T. Eich, S. Devaux, S. Jachmich, S. Brezinsek, G. Maddison, K. McCormick, G.Arnoux, M. Jakubowski, H. Thomsen, A. Huber, F.Militello and JET EFDA contributors

Effect of Ion Mass and Charge on Divertor Heat Load Profiles on JET

Effect of Ion Mass and Charge on Divertor Heat Load Profiles on JET

W. Fundamenski[1], T. Eich[2], S. Devaux[2], S. Jachmich[5], S. Brezinsek[4],
G. Maddison[1], K. McCormick[2], G.Arnoux[1], M. Jakubowski[3], H. Thomsen[3],
A. Huber[4], F.Militello[1] and JET EFDA contributors*

JET-EFDA, Culham Science Centre, OX14 3DB, Abingdon, UK

[1]*EURATOM-CCFE Fusion Association, Culham Science Centre, OX14 3DB, Abingdon, OXON, UK*
[2]*Max-Planck Institut fur Plasmaphysik, IPP-Euratom Association, D-85748 Garching, Germany*
[3]*Max-Planck Institut fur Plasmaphysik, IPP-Euratom Association, Greifswald, Germany*
[4]*Institute fur Plasmaphysik, Forschungszentrum Julich GmbH, Euratom Association, TEC, D-52422, Julich, Germany*
[5]*Association EURATOM-Belgian State, - Ecole Royale Militaire, B-1000 Brussels Belgium*
4Oak Ridge National Laboratory, Oak Ridge, TN 37831, USA
* See annex of F. Romanelli et al, "Overview of JET Results",
(23rd IAEA Fusion Energy Conference, Daejon, Republic of Korea (2010)).*

ABSTRACT.

Inter-ELM and ELM divertor heat loads were measured on JET in dedicated deuterium, hydrogen and helium discharges. Matched triplets (D,H,He) were obtained for different values of magnetic field, plasma current and heating power. In this article, the above experiments are described and the results are presented in terms of empirical scalings of inter-ELM and ELM wetter areas vs engineering parameters. The obtained scalings are then compared with those previously reported in the literature and implications for ITER are tentatively drawn.

1. INTRODUCTION

The key measurement of interest for tokamak power exhaust are the heat load profiles on the outer divertor target (which receives the majority of the average power). The physical mechanism determining these heat loads, both during the inter-ELM and the ELM phases, remains elusive. One way of distinguishing between the various candidate mechanisms is to compare otherwise similar plasma discharges with different main ion mass and charge. In practice, such a comparison can be achieved for hydrogen (H; $A = 1$, $Z = 1$), deuterium (D; $A = 2$, $Z = 1$) and helium (He; $A = 4$, $Z = 2$) plasmas, the first two allowing the comparison of ion mass, the latter two of either mass or charge at constant $A/Z = 2$. By combining all three into a single comparison, the individual effect of A and Z can be inferred.

2. DESCRIPTION OF EXPERIMENTS

Recently, such a comparison was attempted at JET based on a series of dedicated experiments in H, D and He plasmas, with identical magnetic equilibria, i.e. poloidal plasma shapes. In each case, several engineering parameters were varied, albeit with limitations due to pumping and heating constraints in H and He plasmas: the toroidal magnetic field ($1T < B < 3T$), the plasma current (1 MA $< I_p < 3$MA), and hence the edge safety factor ($3 < q_{95} < 5$), the neutral beam heating power (2 MW $< P_{NBI} < 18$MW), the fuelling rate, Γ_0, and hence the line average electron density, n_e, and the corresponding Greenwald fraction ($0.5 < f_{GW} < 1$). From this extensive data set, roughly a dozen good comparison points between H, D and He were identified. Since many of the shots included either power steps or gas fuelling ramps, this translated into roughly two dozen good data points.

The key output of the experiment were the heat load profiles on the outer divertor target. These were calculated from the temperature evolution on the heat bearing septum replacement divertor plate (tile 5), which were measured using an infra-red camera with high spatial (< 2mm along the target) and temporal (~ 80 μs) resolution, allowing separate measurement of inter-ELM, ELM, and time-averaged heat load profiles [1]. The radial width of the heat load profiles will be expressed in terms of the *wetted area* (both inter-ELM and ELM), A_W [m^2], the ELM *deposited energy* on tile 5, $E_{ELM,5}$ [kJ], the ELM *energy load*, ε_{ELM} [kJ/m^2], and the ELM *impact factor*, η_{ELM} [kJm^{-2}s$^{-1/2}$]. The notation, definitions and numerical calculation of these parameters are identical to those used in [2]. The wetted area is related to the integral width, $\lambda_q = \int q(r)dr/q_{max}$, by the expression, $A_W \sim$

$0.8 \times 2\pi R \times \lambda_q \times FX$, where R~2.7 is the major radius and FX is the effective flux expansion (ratio of distances between flux surfaces along the outer target and the outer mid plane), with typically FX ~ 7 for tile 5 @ 2.5MA/2.5T.

3. RESULTS

3.1 DEUTERIUM PLASMAS

As discussed in [1,2], the ELM heat load profiles are generally quite complex. To illustrate this complexity, which generally increases with relative ELM size, the inter-ELM, ELM and average heat load profiles are shown for three deuterium discharges with different relative ELM size, see Figure 1. We first note the apparent narrowness of the inter-ELM profiles, which have widths of ~4 mm mapped to the outer mid-plane, similar to the time averaged values previously reported in [3], based on thermocouple measurements. Since the time averaged widths are only marginally broader than the inter-ELM ones (right frames), the agreement with previously reported measurements would be expected.

We next observed the rapid rise of the ELM power load (left frames), which typically arrives in the ion transit time scale (typically sub-ms on JET). This rapid rise is also found in the far-SOL heat load (middle frames), which explains the broadening of the ELM-integrated profile. This broadening is not smooth but characterized by distinct striations, which are interpreted as foot-prints of plasma filaments ejected during the ELM crash. The temporal evolution of these striations (typically ~ 10) has been studied elsewhere [4]. Their radial extent, and hence the width of the ELM heat load profiles, appears to increase with relative ELM size, up to λ_q^{ELM} ~ 10mm for $\Delta W_{ELM}/W_{dia}$ ~ 9%, or 2.5 times broader than the inter-ELM value of ~4mm.

It should be added that the above ELM behaviour differed substantially between small (convective) ELMs and large (conductive) ELMs: the former showing little or no ELM structure, movement of maximum heat load or broadening with respect to the inter-ELM profiles, while the latter showed significant ELM structure, broadening and movement of peak heat load. In general, the complexity of ELM heat load profiles, their average width and hence power delivered to the far-SOL and the limiters, increased with relative ELM size, as shown in Figure 1.

The measured increase of λ_q^{ELW} with ELM size is consistent with the observation that maximum temperature rise on the outer limiter, as measured by infra-red thermography, decreased with the outer gap (distance between separatrix and outer limiter) and increased roughly as the square root of the normalized (relative) ELM size, see Figure 2, $\Delta T/\Delta W_{ELM} \mu (\Delta W_{ELM}/W_{dia})^{\alpha}$, α ~ 0.35 − 0.65. Hence, larger ELMs were found to deposit a larger fraction of their energy on the first wall, consistent with previous observations, and with divertor measurements [3]. It is worth noting that the radial decay length of the ELM energy load at the limiter is roughly the same in the two cases at ~ 23mm, suggesting the difference in the effective ELM energy width occurs in the near-SOL rather than the far-SOL region [Thomsen10].

2

3.2 DEUTERIUM-HYDROGEN-HELIUM COMPARISON

We next turn the analysis of dedicated D-H-He plasmas in identical magnetic geometry. The divertor heat load profiles for a matched D-H-He triplet with medium sized ELMs ($\Delta W_{ELM}/W_{dia}$ ~ 4-5%) are shown in Figure 3. We note that the inter-ELM profiles are marginally broader in H, and moderately broader in He, compared to the D plasma, with an associated reduction in the peak heat load (bottom frames). Since most of the power reaches the target during the inter-ELM phase, the average profiles were similarly broadened. In contrast, the effect on ELM profiles was less pronounced, with comparable power width in D, H and He plasmas (bottom frames); as a result, the ratio of ELM to inter-ELM widths was smallest in He plasmas. The main difference in the ELM profiles between the three ion species, was the longer power arrival time in He compared, to either D or H (top frames). This increase in the time scale could be expected based on smaller sound speed (square root of mass and lower pedestal temperature and higher pedestal collisionality), as predicted by parallel kinetic modelling of the ELM pulse in the Scrape-off Layer [5,6].

Comparing the inter-ELM wetted areas for the entire database (10 D points, 6 H points and 6 He points), we find mean values of ~0.5 m^2 for D, ~0.55 m^2 for H, and ~0.7 m^2 for He, see Figure 4. Due to an insufficient number of data points for H and He, a multi-variable regression is only meaningful for D data. The result $A_W^{i-ELM,D}$ μ $B^{0.79}I_p^{-0.94}n^{-0.06}P^{0.03}$ μ $B^{-0.15}q_{95}^{0.94}$, indicates the perennial inverse current dependence frequently reported on tokamaks, including JET [7]. Combining data points for all three species, one finds a weaker B scaling (for constant I_p), a weak inverse A scaling, a square root Z scaling, consistent with broader inter-ELM profiles in He plasmas, Figure 5,

$$A_W^{i-ELM} \text{ μ } B^{0.4}I_p^{-0.96}n^{0.16}P^{0.02}A^{-0.13}Z^{0.5} \text{ μ } B^{-0.56}q_{95}^{0.96} \quad (1)$$

We next consider the ELM heat load profiles. The ELM wetted area, maximum energy load and the maximum impact factor, for an average (mean) ELM over 1-2 sec interval around each data point (D, H and He) are plotted vs the ELM deposited energy, Figure 6, and vs the deposited energy normalized by the plasma stored energy, Figure 7 (note that with an inner-outer asymmetry of 2:1, we have $E_{ELM,5}$ ~ $\Delta W_{ELM}/3$). We note that the ELMs are relatively small, with $E_{ELM,5}$ ~ $\Delta W_{ELM}/3$ < 60kJ, $E_{ELM,5}/W_{dia}$ ~ 1%, $\Delta W_{ELM}/W_{dia}$ ~ 3% and $\Delta W_{ELM}/W_{ped}$ ~ 10%. In this range, the ELM wetted area is in the range 0.7-1.3 m^2, is only a weak function of ELM energy and is similar for D, H and He. The maximum energy load is less than 60kJ/m^2, increases roughly linearly with ELM size, and is again comparable for D, H and He. Finally, the maximum ELM impact factor also increases with ELM size, but for $E_{ELM,5}$ > 25kJ, becomes smaller for He than for D or H; this saturation appears to be caused not by a larger wetted area, but by a longer ELM duration, as shown in the lower right frame in Figure 6 and 7. Overall, these four quantities are better ordered by the absolute, rather than relative, ELM size, i.e. Figure 6 rather than Figure 7. Even then, there clearly exist hidden variables (current, field, heating power, fuelling rate, hence pedestal conditions, and A & Z) would

likely improve the ordering of this data.

Finally, we examine the combined D-H-He data for ELM wetted areas plotted vs the best-fit power law scaling, see Figure 5 (left frame),

$$A_W{}^{ELM} \; \mu \; B^{0.2}I_p{}^{-0.78}n^{0.24}P^{0.07} \; E_{ELM,5}{}^{0.06}A^{-0.15}Z^{0.17} \; \mu \; B^{-0.58}q_{95}{}^{0.78} \qquad (2)$$

Comparing with the inter-ELM scaling (1) $A_W{}^{i-ELM} \; \mu \; B^{-0.56}q_{95}{}^{0.96}A^{-0.13}Z^{0.5}$, we find virtually the same B and A scalings, but a somewhat weaker q_{95} (or connection length, $L_{\parallel} \sim \pi q_{95}R$) and Z scalings. Figure 6 also shows the ratio of inter-ELM vs ELM wetted areas, (the inverse of the degree of profile broadening), which scales as

$$A_W{}^{i-ELM}/A_W{}^{ELM} \; \mu \; B^{0.16}I_p{}^{-0.29}n^{-0.07}P^{-0.05}E_{ELM,5}{}^{0}A^{-0.07}Z^{0.41} \; \mu \; B^{-0.13}q_{95}{}^{0.29} \qquad (3)$$

i.e. it exhibits a weak positive dependence on q_{95} and Z. The degree of broadening is largest for D and H (1.5 to 2.5) and is smallest for He (1 to 1.5).

DISCUSSION & CONCLUSION

Not surprisingly, the wetted area scalings (1) and (2) differ from that reported for time-averaged heat load profiles of natural density, high power H-modes [3], $\lambda_q{}^{ave} \; \mu \; B^{-1}q_{95}{}^{0.6}P^{-0.4}n^{0.2}$. This could be caused by a number of factors: the diagnostic technique, the magnetic configuration, the effect of flux expansion (in order to map the target wetted areas to the outer mid-plane – not done here), the time-averaging between of inter-ELM and ELM phases, and the relative scarcity of high power shots data in the present data.

With that caveat in mind, the above results carry several implications for ITER: (i) the previously reported narrow (< 5mm) inter-ELM heat load profiles on JET have been confirmed by IR thermography, (ii) characterization of inter-ELM and ELM heat load profiles in ITER could be performed in both H and He plasmas and then extrapolated to D-T plasmas, correcting for the reported weak A & moderate Z dependence, (iii) the characterization of ELM impact factors may require H (as opposed to He) H-mode plasmas, due to the longer time scales of He ELM energy deposition and smaller degree of ELM profile broadening in He, compared to D and H, plasmas.

REFERENCES

[1]. T. Eich, presented at the 19th PSI Conference, San Diego, May, 2010.

[2]. S. Jachmich, presented at the 19th PSI Conference, San Diego, May, 2010.

[3]. W. Fundamenski, Journal of Nuclear Materials, **390-391** (2009) 10-19.

[4]. S. Devaux, presented at the 19th PSI Conference, San Diego, May, 2010.

[5]. W. Fundamenski, Plasma Physics and Controlled Fusion, **48** (2006) 109-156.

[6]. D. Tskhakaya et al, Contrib. Plasma Physics, **46** (2006) 649.

[7]. W. Fundamenski, Fusion Science and Technology, **53** (2008) 1023-1063.
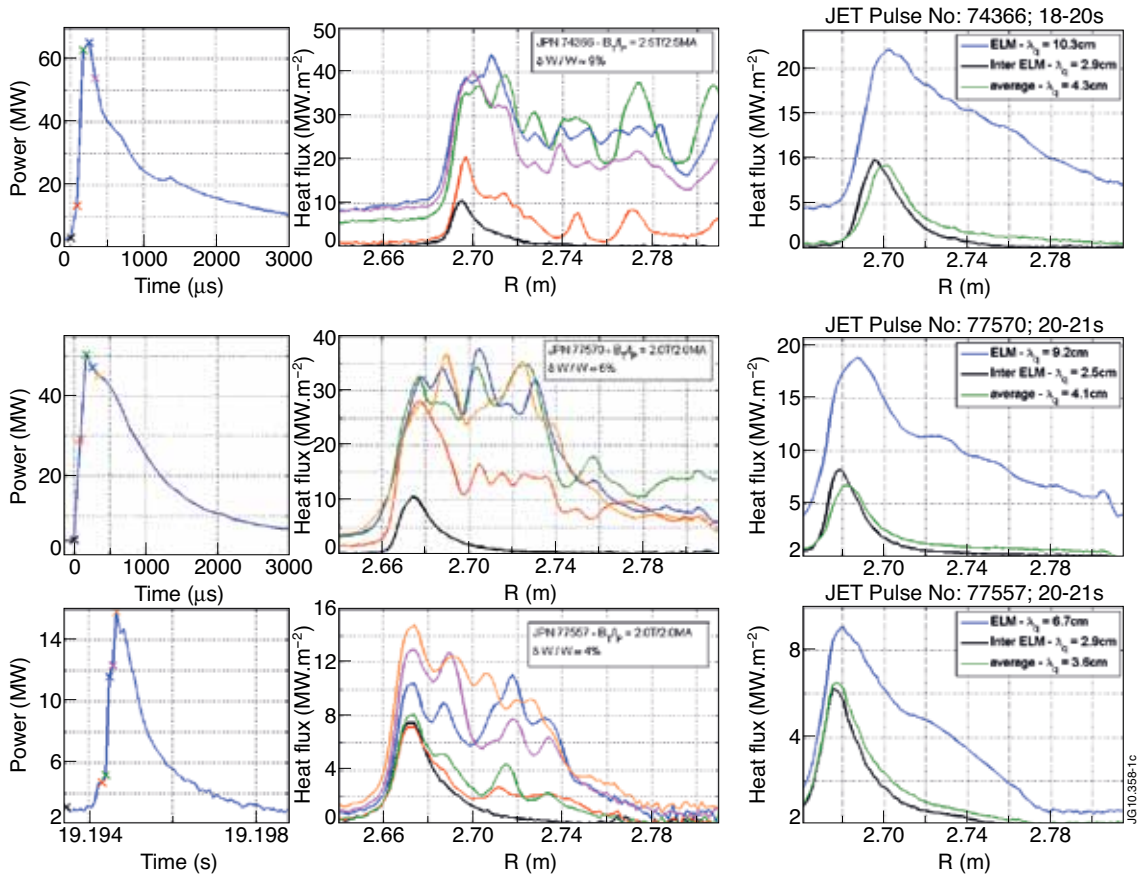
Figure 1: Radial heat load profiles on the outer divertor target for three distinct deuterium discharges with different mean relative ELM size ($\Delta W_{ELM}/W_{dia}$): 9% (top), 6% (middle), 4% (bottom). The left frames show the temporal evolution of the power arriving at the target during the ELM crash. The middle frames show a series of snapshots of the heat load profiles during the course of the ELM crash (as indicated on the left frames). The right frames show radial heat load profiles during the inter-ELM and ELM peak phases, time-averaged over 1-2s, along with average total heat load profile during the same time.
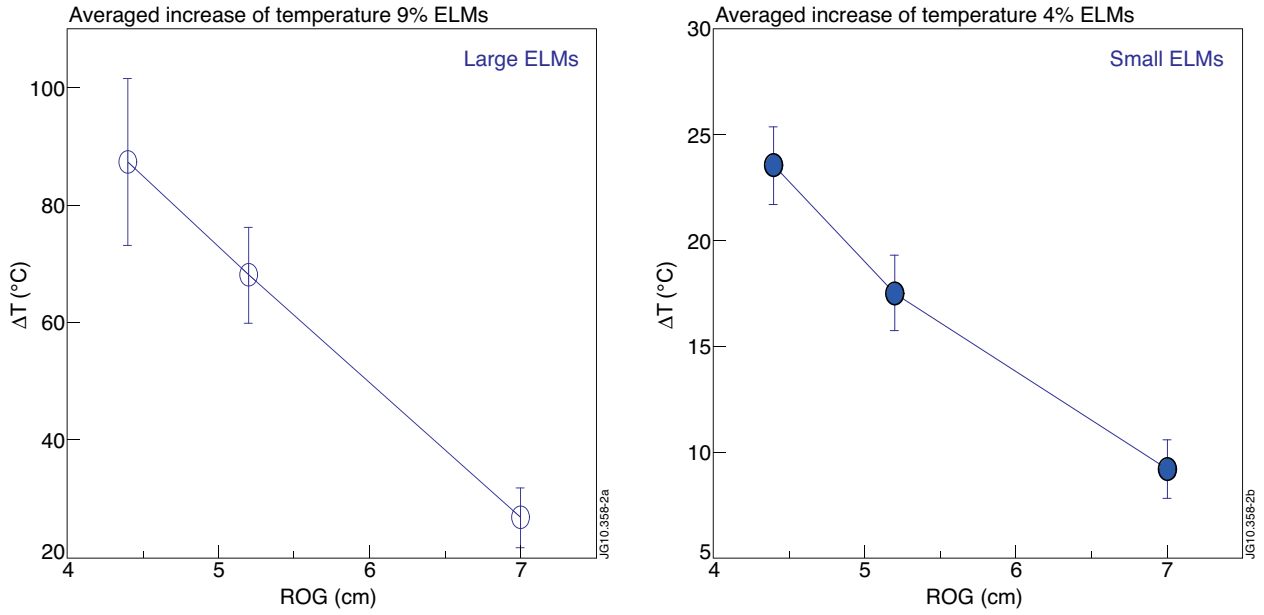
5

Figure 2: ELM heat load interation with outer limiter for two D discharges, with relative ELM size, ($\Delta W_{ELM}/W_{dia}$) of 9% (left) and 4% (right), for different values of the outer gap (ROG)
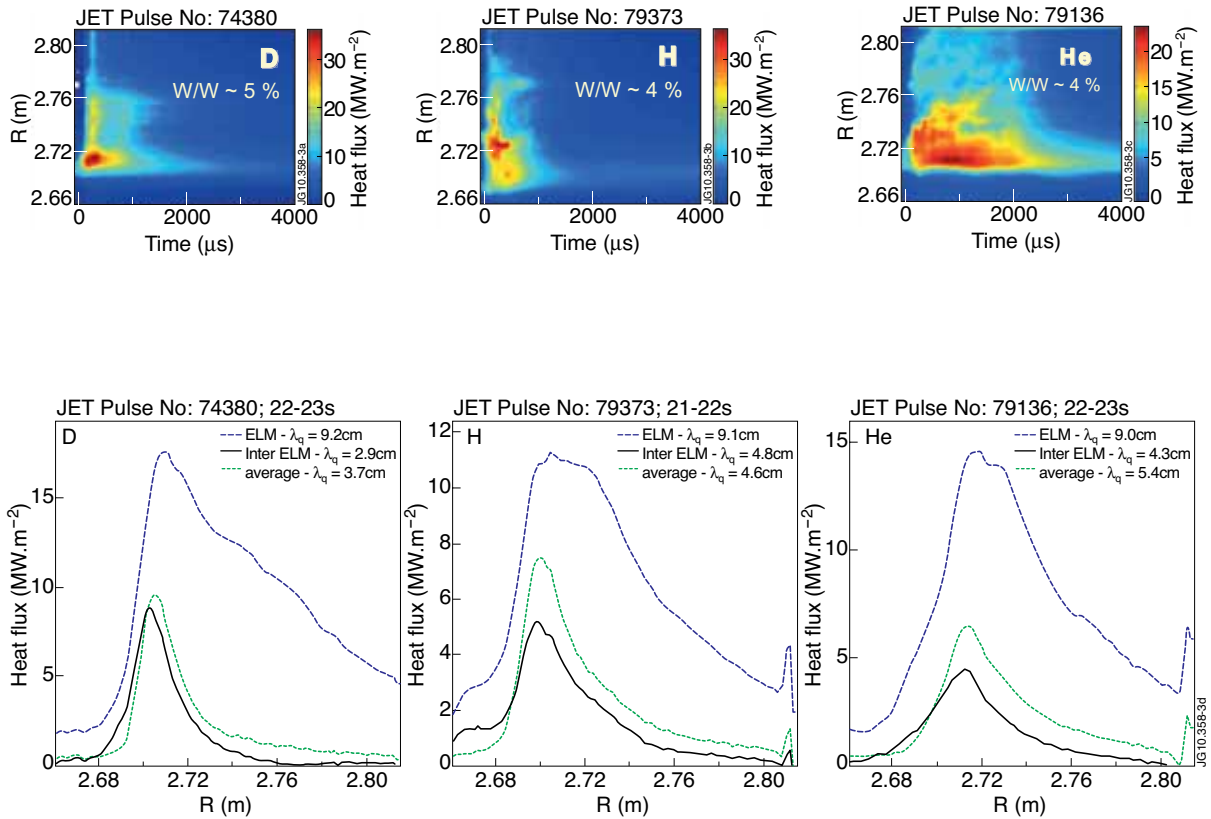

Figure 3: Radial heat load profiles on the outer divertor target in comparable D, H and He plasmas. The bottom frames show inter-ELM, ELM and average profiles and their corresponding integral widths. The top frames show the temporal evolution of the heat load profiles during a typical, medium sized ELMs ($\Delta W_{ELM}/W_{dia} \sim 4$-$5\%$).
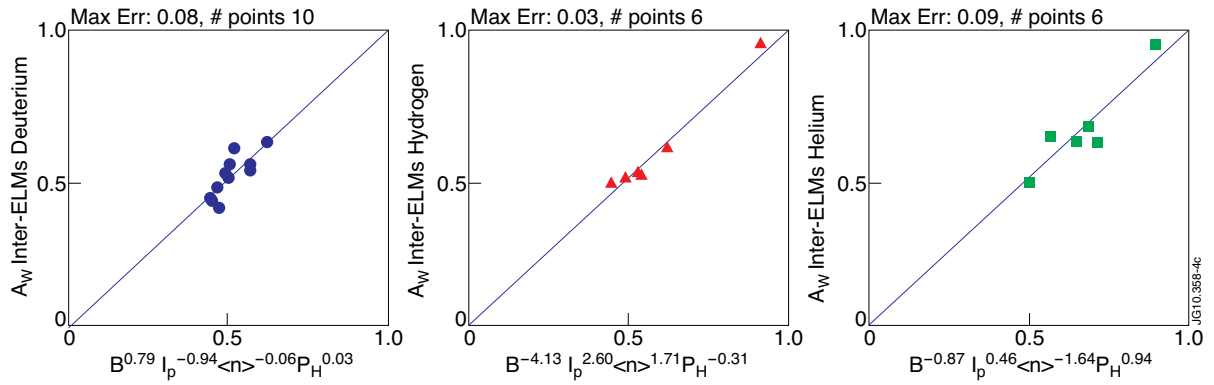
6

Figure 4: IR-measured inter-ELM wetted areas, $A_W^{inter-ELM}[m^2]$ vs best-fit scaling with field, current, density and heating power, for D (left), H (middle) and He (right) plasmas. Note that due to insufficient number of data points (6 points versus 4 scaling variables), clustering in a small range, the stand alone scalings for H and He are unreliable.
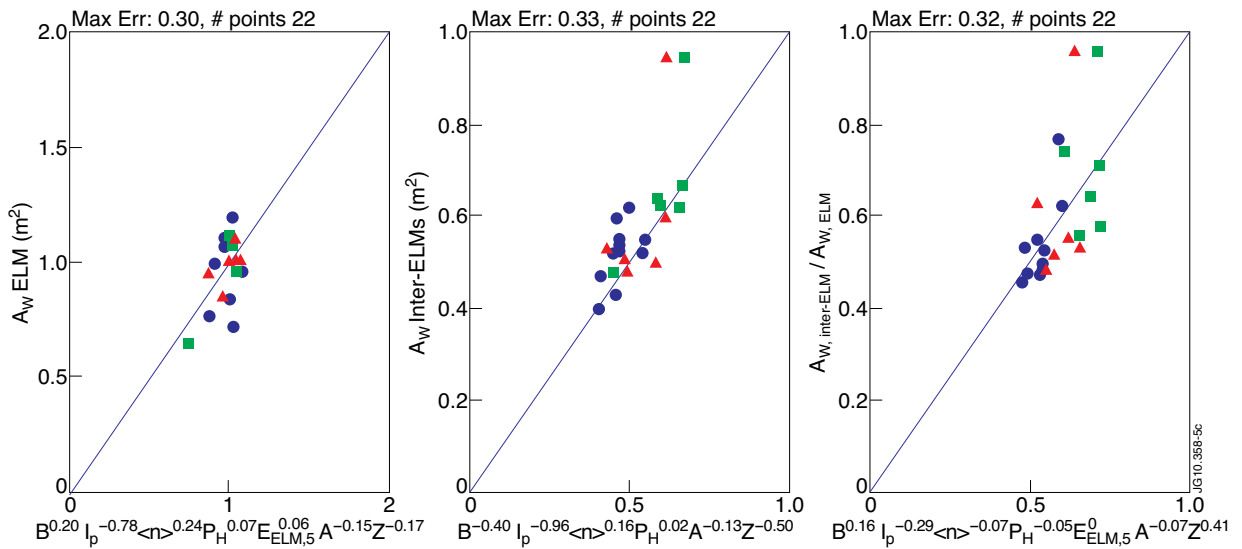

Figure 5: IR-measured wetted areas, $A_W[m^2]$, during ELM (left), inter-ELM (middle) and their ratio (right) vs best-fit scalings with field, current, density, heating power, A and Z (and for ELM quantities also with ELM deposited energy) for all ion species.
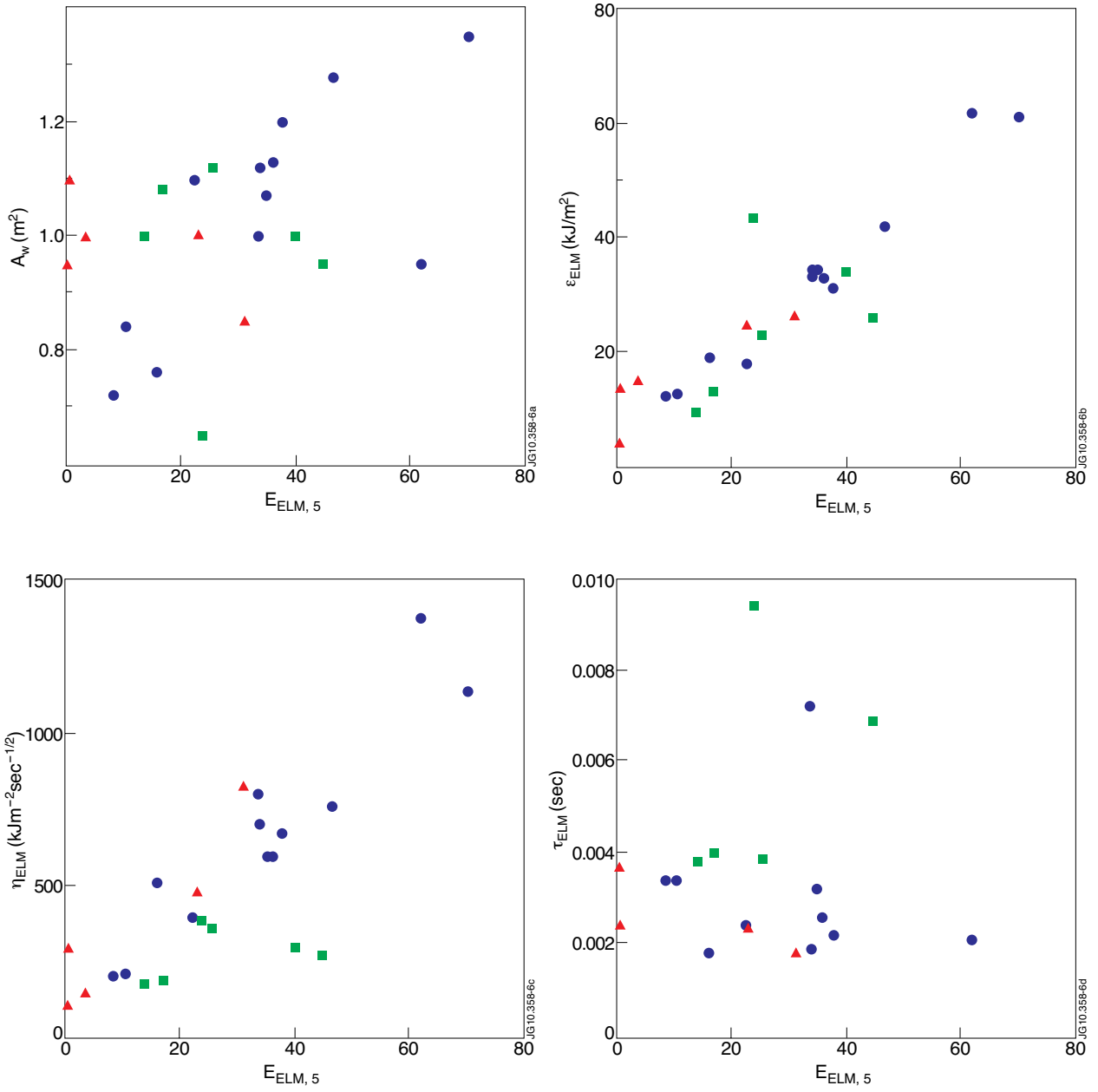
Figure 6: ELM wetted area (top left), maximum ELM energy load (top right) and ELM impact factor (bottom left) and ELM deposition time scale (bottom right) versus ELM deposited energy (kJ).
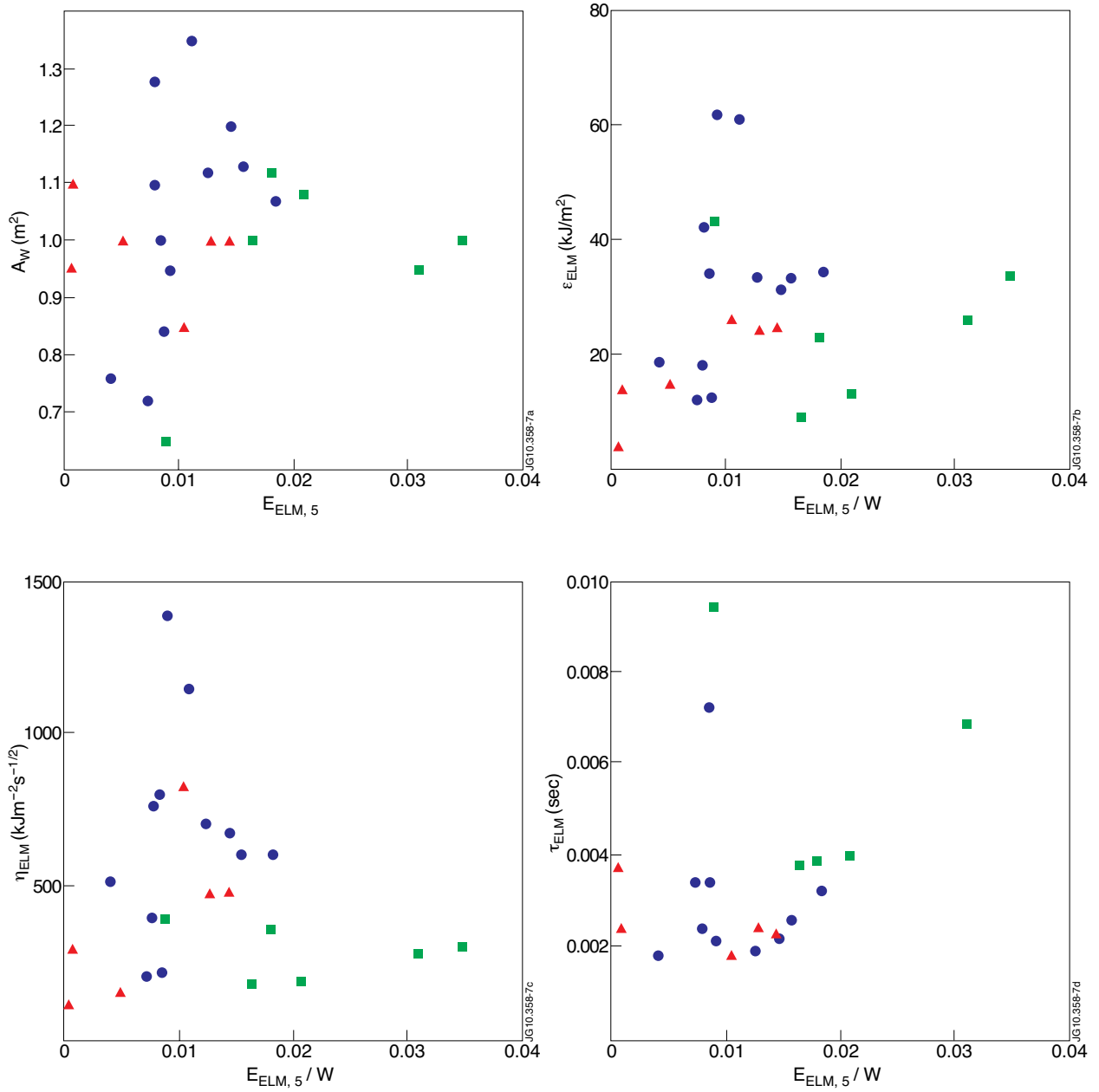
Figure 7: Same as Figure 6, but plotted versus normalized ELM deposited energy.